Temperature-Induced Noise-Insensitive Laser Repeater Station for Optical Frequency Transfer

Ziang Qiu, Zijie Zhou, Liang Hu, *Member, IEEE*, Jiao Liu, Guiling Wu, *Member, IEEE*, Jianping Chen, Xiang Zhang, Ruifang Dong, Tao Liu, and Shougang Zhang

***Abstract*— We report on the realization of a temperature-induced noise-insensitive laser repeater station (TiLRS), which can effectively remove the annoying out-of-loop phase noise existing in the conventional laser repeater station (LRS). TiLRS is able to achieve the same capability as the conventional LRS including power amplification, signal regeneration, and phase noise compensation. More importantly, based on the out-of-loop noise inline detection and the active noise compensation (ANC) setup, our system gets rid of the need for the sophisticated temperature control system and precise out-of-loop path matching. In addition, we also design the temperature-induced noise-insensitive local station (TiLS) and remote station (TiRS) as well as the modified two-way comparison (MTWC) method for the instability evaluation. The phase-temperature coefficient of the proposed cascaded system can achieve 9.1 as/K, which is three orders of magnitude lower than the same configuration suffering from the out-of-loop noise and is the best value reported so far for the fiber-optic interferometer. We experimentally demonstrate the cascaded optical frequency transfer system by using one TiLRS connecting the 460-km commercial fiber link with the fractional frequency instability of about 1.01×10^{-15} at 1 s and 1.20×10^{-19} at 10 000 s. This technology paves the way for the optical frequency transfer networks with high accuracy, high robustness, and low temperature sensitivity.**

***Index Terms*— Active noise compensation, metrology, optical clock, optical frequency transfer, temperature-induced noise-insensitive laser repeater station (TiLRS).**

Received 12 November 2024; revised 16 February 2025; accepted 5 April 2025. Date of publication 16 April 2025; date of current version 7 May 2025. This work was supported in part by the National Natural Science Foundation of China (NSFC) under Grant 62375167 and Grant 62120106010, in part by Zhejiang provincial Key Research and Development Program of China under Grant 2022C01156, and in part by the National Science Foundation of Shanghai under Grant 22ZR1430200. The Associate Editor coordinating the review process was Dr. Gordon Shaw. *(Corresponding author: Liang Hu.)*

Ziang Qiu and Zijie Zhou are with the State Key Laboratory of Photonics and Communications, Department of Electronic Engineering, Shanghai Jiao Tong University, Shanghai 200240, China (e-mail: 21008563@sjtu.edu.cn; zhouzijie@sjtu.edu.cn).

Liang Hu, Jiao Liu, Guiling Wu, and Jianping Chen are with the State Key Laboratory of Photonics and Communications, Department of Electronic Engineering, Shanghai Jiao Tong University, Shanghai 200240, China, and also with the SJTU-Pinghu Institute of Intelligent Optoelectronics, Jiaxing Time-Transfer Photoelectric Company Ltd., Pinghu 314200, China (e-mail: liang.hu@sjtu.edu.cn; liujiao@sjtu.edu.cn; wuguiling@sjtu.edu.cn; jpchen62@sjtu.edu.cn).

Xiang Zhang, Ruifang Dong, Tao Liu, and Shougang Zhang are with the National Time Service Center, Chinese Academy of Sciences, Xi'an 710600, China, also with the University of Chinese Academy of Sciences, Beijing 100049, China, and also with the Key Laboratory of Time and Frequency Standards, Chinese Academy of Sciences, Xi'an 710600, China (e-mail: zhangxiang@ntsc.ac.cn; dongruifang@ntsc.ac.cn; taoliu@ntsc.ac.cn; szhang@ntsc.ac.cn).

Digital Object Identifier 10.1109/TIM.2025.3561397

I. Introduction

With the rapid development of optical frequency standard technology, optical atomic clocks have achieved an unprecedented accuracy about 1 part in 10^{-18}, an improvement of two orders and more over the microwave atomic clocks [1], [2]. Currently, high-performance optical clock networks are also widely used in time and frequency metrology [3], [4], radio astronomy [5], [6], gravitational-wave detection [7], and testing of fundamental physics [8]. However, optical atomic clocks are not suitable for large-scale distributed applications since they are sensitive to the environment and large in size. Optical frequency transfer technology is the key to advancing the practicality of optical atomic clocks, enabling users in different locations to share the same high-performance source. Taking advantage of the excellent characteristics of optical fibers such as low loss and high interference immunity [9], high-precision optical frequency transfer via optical fibers has been widely investigated and employed [4], [5], [7], [10], [11].

Unfortunately, in directly linked fiber-optic frequency transfer, the received signal to noise ratio (SNR) will decrease due to the attenuation in the fiber link when the transfer distance increases. This problem can be solved by using the bidirectional erbium-doped fiber amplifiers (Bi-EDFAs) [5], [12]. However, the amplified spontaneous emission (ASE) noise and the double Rayleigh scattering (DRS) noise in the fiber link will reduce the SNR at the receiving site, which will cause the frequent cycle slips and lock-losing [13]. To avoid this, the optimum gain is usually limited to about 13–20 dB [14], [15]. More importantly, the control bandwidth of the noise compensation system is restricted by $1/4\tau_0$ [16], where τ_0 is the one-way fiber propagation delay. To overcome these limitations, a number of cascaded optical frequency transfer techniques are proposed, including the EDFA-based repeater station (ERS) [17], the laser injection locking-based repeater station (ILRS) [18], [19], and the laser repeater station (LRS) [20], [21], [22], [23]. The typical cascaded setup, as shown in Fig. 1(a), consists of a local station (LS) for

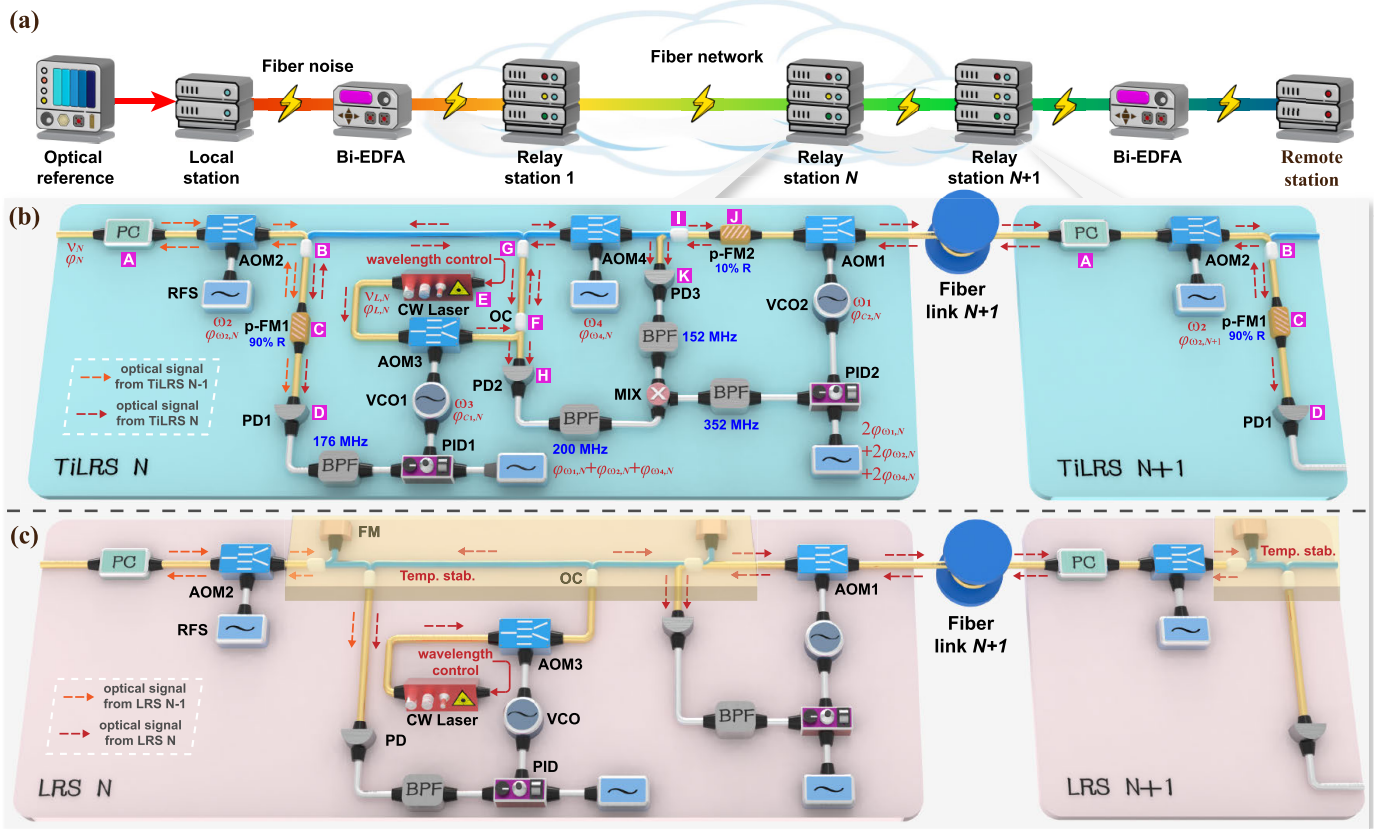

Fig. 1. (a) Schematic of the conventional cascaded optical frequency transfer system, here Bi-EDFAs between each station are used for the bidirectional amplification of the optical signals. (b) Schematic of the proposed TiLRS. PC: polarization controller, AOM: acousto-optic modulator, OC: optical coupler, p-FM: partial Faraday mirror, RFS: radio frequency source, PD: photodetector, BPF: bandpass filter, PID: proportional-integral-derivative controller, VCO: voltage-controlled oscillator, and MIX: frequency mixer. (c) Schematic of the conventional LRS [20], [21]. FM: Faraday mirror. The blue cylinders represent the out-of-loop paths, and the orange and red dotted lines with an arrow represent the propagation direction of the optical frequency signal.

transmitting the optical frequency signal, the repeater stations for regenerating and amplifying the optical frequency signal, and a remote station (RS) for receiving the phase-stabilized optical frequency signal. The ERSs use two-stage EDFAs to achieve amplification of the received optical frequency signal and the phase noise introduced by the EDFAs can be actively canceled by optical phase locking. They enable high-gain optical frequency amplification and get rid of the laser sources but suffer from greater noises compared with the ILRSs and LRSs. The ILRSs realize the optical frequency signal amplification by means of the injection locking process. The received signal is used as the seed to inject into the laser in the repeater station to realize the amplification. However, the ILRSs need additional electrooptic modulators (EOMs) or acousto-optic modulators (AOMs) to increase the tuning range of the intensity. The LRSs lock the local regenerative laser to the phase of the received signal to realize the regeneration feature. The output signal has the same phase noise and instability characteristics as the received signal, which can be used as the optical source for the next link.

The typical optical frequency transfer system is usually realized by the unbalanced Michelson interferometers. With the help of the Faraday mirrors (FMs), the interferometer leaves one part of the optical frequency signal as the reference at the LS, forming the reference arm. The other part is sent to the fiber link and reflected back to the LS by the FM at the RS, forming the transmission arm. Due to the pigtails of the fiber-optic devices, there exist non-reciprocal paths both in the reference arm and the transmission arm, which results in the interferometer asymmetry. These asymmetric parts are called the out-of-loop paths, and they will introduce phase noise when perturbations such as temperature fluctuations and vibrations occur [16], [24]. As demonstrated in [25], the phase variations caused by temperature fluctuation $\Delta T(t)$ with an out-of-loop path of L can be expressed as follows:

$$\Delta\varphi(t) = \frac{\omega L}{c}(\alpha_n + n_e\alpha_\Lambda)\Delta T(t) \tag{1}$$

where ω is the angular frequency of the optical signal, c is the propagation speed of the optical signal, $n_e \approx 1.468$ is the refractive index of the typical single-mode fiber, $\alpha_n \approx 1.03 \times 10^{-5}$/K (room temperature) and $\alpha_\Lambda \approx 5.5 \times 10^{-7}$/K (room temperature) are the thermo-optic coefficient [26] and fiber linear expansion coefficient [27] of the single-mode fiber, respectively. Equation (1) demonstrates that the out-of-loop paths will have a significant effect on the instability of the optical frequency transfer at various levels depending on the length L and the characteristics of the temperature fluctuations. After transforming the phase error into time error, a linear representation of the time error versus temperature variation

can be obtained as follows:

$$\Delta\tilde{\varphi}(t) = \frac{L}{c}(\alpha_n + n_e\alpha_\Lambda)\Delta T(t) = \gamma\Delta T(t) \quad (2)$$

where γ is defined as the phase-temperature coefficient [28]. For a 1-m fiber link transmitting an optical signal with a frequency near 193 THz at room temperature, $\gamma \approx 37$ *f*s/K. Fig. 1(c) shows the configuration of a conventional LRS demonstrated in [20], [21], and [22], where the blue highlighted parts are the out-of-loop paths of the interferometer. Assuming that the external ambient temperature fluctuation is approximated as sinusoidal fluctuations with a period of 3600 s and the peak-to-peak value is about 1 K, the modified Allan deviation (MDEV) will be as high as 1×10^{-19} at 1800 s if the length of these out-of-loop paths is about 10 cm.

Although the system instability can be improved by k times by equally dividing the whole fiber link into k segments if the phase noise is uniformly distributed [21], the out-of-loop noise will be linearly increased with the increase of the LRSs. Assuming that $k-1$ LRSs equally divide the fiber link into k segments and the phase noise power spectral density (PSD) caused by the out-of-loop path in the Nth LRS is $S_{\mathrm{op},N}(\omega)$, then the residual phase noise PSD of the whole link can be expressed as follows:

$$S_{r,\mathrm{fiber}}(\omega) = \frac{\omega^2\tau^2}{3k^2}S_{\mathrm{fiber}}(\omega) + \sum_{N=1}^{k-1} S_{\mathrm{op},N}(\omega) + S_{\mathrm{op},L}(\omega) + S_{\mathrm{op},R}(\omega) \quad (3)$$

where τ and $S_{\mathrm{fiber}}(\omega)$ represent the one-way propagation delay and the phase noise PSD of the entire fiber link, respectively. $S_{\mathrm{op},L}(\omega)$ and $S_{\mathrm{op},R}(\omega)$ represent the out-of-loop noise PSD of the LS and RS. To mitigate the effects of the out-of-loop noise, the out-of-loop paths need to be exactly matched in length or to be kept as short as possible [29]. Although they can be shortened by fusion splicing the fibers between the optical components, the length is difficult to be reduced to a few centimeters due to the fusion splicer's constraint. Therefore, according to (1), the conventional LRSs inevitably require precise temperature control with temperature fluctuations of not more than 0.01 K to ensure the long-term instability in the order of 10^{-21} under our assumptions, which will greatly increase the system complexity. Another way to reduce the out-of-loop noise is to use free-space interferometers since the refractive index in the air is three orders of magnitude lower than that in the optical fibers [30]. However, free-space interferometers are susceptible to uncertainty contributions resulting from optics movements and the related beam pointing variations [31], [32]. Previous study has demonstrated the feasibility of combining active temperature stabilization with free-space interferometer in the LRSs, thereby achieving nearly full mitigation of temperature-related effects [33]. To further suppress the potential temperature-related effects, post-processing of phase data considering temperature fluctuations is still required [34]. Additionally, the integrated interferometer on a single chip is also an effective way to shorten the out-of-loop paths as implemented in [35], which has the advantages of small size and short out-of-loop paths, and the out-of-loop path is easy to be matched in length. It has been demonstrated in our previous work [36] that the noise floor of the chip-based system is almost one to two orders of magnitude lower than the temperature-stabilized fiber interferometer [37]. However, coupling between chip-based interferometers and optical fibers will introduce non-negligible additional insertion loss, which limits their application.

In this article, we propose a cascaded optical transfer scheme including the temperature-induced noise-insensitive laser repeater stations (TiLRSs), temperature-induced noise-insensitive local station (TiLS), and remote station (TiRS) as well as a modified end-to-end test (ET) method which avoids introducing additional out-of-loop paths. With the help of partial FMs (p-FMs), the out-of-loop noise of the interferometer can be detected inline and suppressed together with the fiber link-introduced phase noise by the active noise compensation (ANC) setup. The TiLS, TiLRS, and TiRS are free from temperature control; the phase-temperature coefficient of our proposed interferometer structure is three orders of magnitude lower than the conventional fiber-optic structures [28], [29], [38]. The test results show that, for the 460-km cascaded commercial field fiber link, our proposed cascaded system with one TiLRS has a fractional frequency instability of 1.01×10^{-15} at the integration time of 1 s and 1.20×10^{-19} at the integration time of 10 000 s.

II. Principle

A. Principle of the TiLRS

In the cascaded transfer system, the purpose of the TiLRSs mainly concerns three aspects, including power amplification, signal regeneration, and phase noise compensation. Different from the conventional LRS, our proposed TiLRS also has the ability of the out-of-loop noise compensation during the ANC setup. For the construction of the TiLRS, we choose p-FMs instead of the conventional FMs, which are capable of reflecting a portion of the received signal on one side and transmitting the other, while rotating the polarization of the signal by 45° for a single pass. Such inline configuration can incorporate the paths connected to the FMs shown in Fig. 1(c) into the loop, thus, minimizing the out-of-loop path in the interferometer. What is more, by carefully selecting the appropriate frequency during the locking process, the proposed TiLRSs are free from the radio frequency (RF) noise introduced by the time-base mismatch.

The regeneration of the received optical frequency signal is achieved by the front part of the TiLRS. Assume that the angular frequency and phase of the optical frequency signal received in the Nth TiLRS are ν_N and φ_N, respectively. After passing through AOM2 (upshifted mode, +1 order) working at an angular frequency of ω_2 and p-FM1, the majority of the signal is reflected back toward the front link, while a minor proportion entering photodetector1 (PD1), which can be expressed as follows:

$$E_1 \propto \cos\left[(\nu_N + \omega_2)t + \varphi_N + \varphi_{CD,N}\right] \quad (4)$$

where $\varphi_{mn,N}$ is the phase noise introduced by the fiber segment from point m to point n in the Nth TiLRS. Considering the

reciprocity of the transmission paths, there is $\varphi_{mn,k} = \varphi_{nm,k}$. Here, we ignore the phase noise introduced in points A to C, since it can be compensated by the link locking process at the $N-1$th station as the in-loop path, and this will be demonstrated in the subsequent derivation. PD1 is employed for detecting the frequency difference and phase difference between the received signal and the local reference signal from the regenerative laser, and the beatnote signal can be written as follows:

$$E_2 \propto \cos\big[(\nu_{L,N} - \omega_3 - \nu_N - \omega_2)t + \varphi_{L,N} + \varphi_{\mathrm{EC},N} + \varphi_{c1,N} - \varphi_N\big] \quad (5)$$

where $\nu_{L,N}$ and $\varphi_{L,N}$ are the angular frequency and phase of the regenerative laser in the Nth TiLRS, ω_3 is the driving angular frequency of AOM3 (downshifted mode, -1 order), and $\varphi_{c1,N}$ is the correctional phase shifts by controlling the frequency of the voltage-controlled oscillator1 (VCO1) driving for AOM3. The beatnote is then sent to the phase locked loop (PLL) consisting of proportional-integral-derivative controller1 (PID1) and VCO1. Before the locking process, the wavelength of the regenerative laser is regulated in close proximity to that of the received signal through temperature tuning control together with the external piezo-electric transducer (PZT) [not drawn in Fig. 1(b)], thereby ensuring that the beatnote signal falls within the locking bandwidth of the PLL [21]. When the laser wavelength is stabilized, the optical frequency signal (whose angular frequency is $\nu_{L,N} - \omega_3$) after passing through AOM3 is locked to a negative offset of $\omega_1+\omega_2+\omega_4$ compared with the received signal (whose angular frequency is $\nu_N+\omega_2$) to eliminate the effect of the RF noise, where ω_1 and ω_4 are the driving angular frequency of AOM1 (upshifted mode, $+1$ order) and AOM4 (upshifted mode, $+1$ order). When the loop is in-lock, the following relationship can be obtained:

$$\begin{aligned} \nu_{L,N} - \omega_3 &= \nu_N + \omega_2 - (\omega_1 + \omega_2 + \omega_4) \\ \varphi_{L,N} + \varphi_{\mathrm{EC},N} + \varphi_{c1,N} &= \varphi_N - \varphi_{\omega_1,N} - \varphi_{\omega_2,N} - \varphi_{\omega_4,N} \end{aligned} \quad (6)$$

where $\varphi_{\omega_i,N}$ represents the RF phase noise from the RF source (RFS) with an angular frequency of ω_i. Thus, if the loop is in-lock, the PLL will regenerate a high power optical frequency signal, phase-coherent to the incoming signal.

Although some out-of-loop paths can be eliminated by the p-FMs, the fibers indicated by the blue cylinders in Fig. 1(b) still introduce non-reciprocal phase noise. Such temperature-induced noise will deteriorate as indicated in (3), if it is not compensated. Therefore, we propose an inline out-of-loop noise detection method to extract the out-of-loop noise information shown by the blue path through an additional AOM (AOM4) and PD (PD2). After passing through AOM3 and an optical coupler (OC) (point F), the optical frequency signal from the regenerative laser is then divided into two parts by the OC at point G. One part passes through another OC (point B) and is reflected by p-FM1 to PD2. The other part is reflected by p-FM2 and enters into PD2 after passing through AOM4. Consequently, the angular frequency of the beatnote obtained in PD2 is $2\omega_4$ and can have an expression given as follows:

$$E_3 \propto \cos(2\omega_4 t + 2\varphi_{GJ,N} - 2\varphi_{\mathrm{CG},N} + 2\varphi_{\omega_4,N}). \quad (7)$$

The locked regenerative laser in the Nth TiLRS sends the optical frequency signal to the $N+1$th TiLRS and the phase noise $\varphi_{\mathrm{fp},N+1}$ introduced by the $N+1$th fiber link can be detected in PD4. When the regenerative signal passes through AOM4, a small portion is reflected by p-FM2 to PD3, as the reference signal, which can have the following form:

$$E_4 \propto \cos\big[(\nu_N - \omega_1)t + \varphi_N - \varphi_{\omega_1,N} - \varphi_{\omega_2,N} - \varphi_{\mathrm{GC},N} + \varphi_{\mathrm{GI},N} + 2\varphi_{IJ,N} + \varphi_{IK,N}\big]. \quad (8)$$

The rest of the signal enters the $N+1$th fiber link after passing through AOM1, and reaches p-FM1 after passing through AOM2 in the $N+1$th TiLRS, which can be depicted as follows:

$$E_5 \propto \cos\big[(\nu_N + \omega_2)t + \varphi_N - \varphi_{\omega_1,N} - \varphi_{\omega_1,N} - \varphi_{\mathrm{GC},N} + \varphi_{GJ,N} + \varphi_{c2,N} + \varphi_{\mathrm{fp},N+1} + \varphi_{\mathrm{ac},N+1} + \varphi_{\omega_2,N+1}\big] \quad (9)$$

where $\varphi_{c2,N}$ is the correctional phase shift by controlling the frequency of the VCO2 driving for AOM1. With the help of p-FM1 in the $N+1$th TiLRS, most of the signal is reflected back into PD3 in the Nth TiLRS, and the beatnote with the reference signal E_4 can be denoted as follows:

$$E_6 \propto \cos\big[2(\omega_1 + \omega_2)t + 2\varphi_{c2,N} + 2\varphi_{\mathrm{fp},N+1} + 2\varphi_{\mathrm{ac},N+1} + 2\varphi_{\omega_2,N+1}\big]. \quad (10)$$

It is worth mentioning that there is an additional all-pass p-FM between p-FM2 and AOM1 [not drawn in Fig. 1(b)] to ensure that the two optical frequency signals just before the PDs in the TiLRS have the same polarization to obtain the maximum power of the beatnote. In addition, we add the automatic polarization controller (PC) device proposed in our previous work [37] to the receiving site of the TiLRS to deal with the random polarization changes caused by the fiber links. By means of the gradient descent algorithm, the power of the beatnote signal used for noise compensation can be automatically optimized to the maximum.

To compensate for the out-of-loop noise and the fiber link-introduced phase noise, we mix E_6 with E_3 and the upper sideband signal is obtained and can be given by the following:

$$E_7 \propto \cos\big[2(\omega_1 + \omega_2 + \omega_4)t + 2\varphi_{c2,N} + 2\varphi_{\mathrm{fp},N+1} + 2\varphi_{\omega_4,N} + 2\varphi_{GJ,N} - 2\varphi_{\mathrm{CG},N} + 2\varphi_{\mathrm{ac},N+1} + 2\varphi_{\omega_2,N+1}\big]. \quad (11)$$

Similarly, during the ANC setup, we lock E_7 to the RFS with the angular frequency of $2(\omega_1+\omega_2+\omega_4)$. The phase error is detected via PID2, and by tuning the control voltage of VCO2, the steady-state error is canceled, resulting in the following:

$$\varphi_{c2,N} + \varphi_{\mathrm{fp},N+1} = \varphi_{\omega_1,N} + \varphi_{\omega_2,N} - \varphi_{GJ,N} + \varphi_{\mathrm{CG},N} - \varphi_{\mathrm{ac},N+1} - \varphi_{\omega_2,N+1}. \quad (12)$$

By substituting the equation into E_5, the phase stable optical signal without the out-of-loop noise can be written

as follows:

$$E_8 \propto \cos[(\nu_N + \omega_2)t + \varphi_N]. \tag{13}$$

Equation (13) demonstrates that the angular frequency and phase of the optical frequency signal to be transmitted are regenerated at the front part of the $N+1$th TiLRS. Furthermore, all the RF noise generated by the RFSs in the Nth TiLRS is entirely eliminated, thereby ensuring that the system can operate with an independent time-base without affecting the instability of the output optical frequency signal.

B. Cascaded Transfer System and the End-to-End Test Method

Fig. 1(a) shows the typical schematic of the cascaded system for optical frequency transfer. The optical reference at the LS is transmitted to the RS via the fiber links and a number of repeater stations. The power degradation introduced by the segmented fiber link can be compensated by the Bi-EDFAs. Fig. 2(a) shows the conventional setup of the LS and RS for optical frequency transfer as well as the end-to-end test. Similarly, out-of-loop paths also exist in the LS and RS (blue highlighted lines) and should be strictly temperature controlled.

Analogously, we realize the TiLS and TiRS by optimizing the interferometer structure with the p-FMs, which is shown in Fig. 2(b). In the TiLS, p-FM3 reflects part of the optical reference and transmits the other to the fiber network, which will be returned back to the PLL by the same path with the help of p-FM4 in the TiRS. Therefore, the out-of-loop paths in the conventional LS and RS can be eliminated, and the TiLS and TiRS do not need any temperature control process.

When it comes to the ET process, the LS and RS are typically deployed at one same site and connected with an additional short fiber, as shown in Fig. 2(a). Thus, the reference signal (blue arrows) from the LS can be transmitted to the RS via the short fiber to phase detect with the received optical frequency signal transmitted through the fiber link (purple arrows). Similarly, the signal received by the RS can be transmitted back to the LS. Assuming that the short fiber-introduced phase noise is $\varphi_{sp,1}$ and the residual phase noise received at the RS is $\varphi_{res,1}$, the two ET signals (ET1 and ET2) obtained at the LS and RS can have a phase of $\varphi_{res,1}+\varphi_{sp,1}$ and $\varphi_{res,1}-\varphi_{sp,1}$, respectively. By performing simple post-processing calculations, the undesired phase noise introduced by the short fiber can be effectively eliminated. Such ET method is called the two-way optical frequency comparison (TWC) method [38], [39]. However, as the blue highlighted lines demonstrated, it will inevitably introduce additional out-of-loop paths. To solve this problem, as Fig. 2(b) shows, we design a modified TWC (MTWC) method based on the proposed structure.

Taking the ET between the TiLS and TiRS as an example, the two stations are connected with a short fiber and AOM5 working at an angular frequency of ω_5 (downshifted mode, -1 order), as Fig. 2(b) shows. With the help of p-FM3 and p-FM4, the out-of-loop paths can be incorporated into the loop since the optical frequency signal can bidirectionally pass through the short fiber and AOM5. The optical spectrum

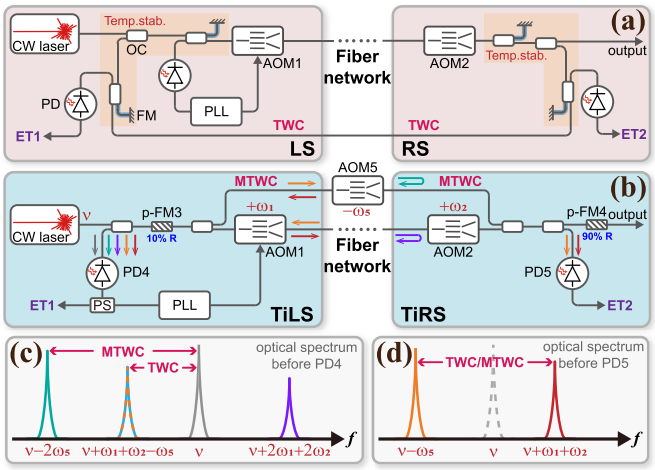

Fig. 2. (a) Schematic of the LS and RS in the conventional cascaded system together with the conventional TWC method [38], [39] for the end-to-end test (ET). OC: optical coupler, FM: Faraday mirror, AOM: acousto-optic modulator, PD: photodetector, and PLL: phase locked loop. The fibers marked by the blue highlighted lines represent the out-of-loop paths. (b) Schematic of the TiLS and TiRS together with the MTWC method suitable for our proposed cascaded system. p-FM: partial Faraday mirror and PS: power splitter. (c) Optical spectrum diagram just before (b) PD4 in the TiLS and (d) PD5 in the TiRS.

diagrams just before PD4 at the TiLS and PD5 at TiRS are shown in Fig. 2(c) and (d); here we have omitted the spectrum of multiple reflections for brevity. It is worth noting that, the signal that passes through the fiber link and is reflected back to the TiLS through the short fiber (red arrows) has the same angular frequency $(\nu+\omega_1+\omega_2-\omega_5)$ with the signal that passes through the short fiber first and is reflected back through the fiber link (orange arrows). Thus, at the TiLS, it is unreasonable to still choose the beatnote between the reference and the TiRS received signal for the system performance evaluation, due to the presence of frequency aliasing. To eliminate the undesired short fiber-introduced phase noise during the ET process, we choose the beatnote between the reference (gray arrow) and the round-trip signal through the short fiber (cyan arrows) as the ET signal (ET1) at the TiLS, which can be expressed as follows:

$$E_9 \propto \cos(2\omega_5 t - 2\varphi_{sp,2}) \tag{14}$$

where $\varphi_{sp,2}$ is the phase noise introduced by the short fiber and AOM5. Here and in the subsequent derivation, we ignore the phase noise introduced by the pigtails of the p-FMs and OCs since they are either in-loop or can be passively eliminated during the phase detection process. The other ET signal (ET2) is obtained by PD5 at the TiRS, which is the beatnote between the signal through the fiber link (red forward arrow) and the signal through the short fiber (orange forward arrow), and can have the following form:

$$E_{10} \propto \cos[(\omega_1+\omega_2+\omega_5)t + \varphi_{res,2} - \varphi_{sp,2}] \tag{15}$$

where $\varphi_{res,2}$ is residual phase noise received at the TiRS. To eliminate $\varphi_{sp,2}$, ET1 is divided by a factor of two and mixed with ET2. Therefore, the lower sideband signal can be used for evaluating the system performance without any additional

short fiber-introduced noise. In addition, a similar structure can be used in each TiLRS for the ET.

III. Experiment Setup and Results

A. Experiment Setup

We have demonstrated the proposed scheme with the TiLS, TiLRSs, and TiRS by using the setup as shown in Figs. 1(b) and 2(b). The optical reference is a narrow-linewidth laser (NKT X15) at a frequency near 193 THz with a linewidth of 100 Hz, which can support coherent optical frequency transfer more than one-thousand kilometers. In addition, it also acts as the regenerative laser in each TiLRS. Here we set $\omega_1 = 2\pi \times 39$ MHz, $\omega_2 = 2\pi \times 37$ MHz, $\omega_3 = 2\pi \times 100$ MHz, and $\omega_4 = 2\pi \times 100$ MHz. With this configuration, the center frequency of the BPFs just after PD1, PD2, PD3, and MIX is 176, 200, 152, and 352 MHz, respectively. It is worth mentioning that since we use the fiber laser as the regenerative laser and the PZT driving for the laser has limited frequency tuning bandwidth, we add AOM3 to expand it. The selected p-FM1 and p-FM4 have 90% reflectivity for the bidirectional transmission in the fiber link, while p-FM2 and p-FM3 require only 10% reflectivity for the reference signal. The driving angular frequency of AOM5 ω_5 used for the ET is set to be $2\pi \times 100$ MHz. Thus, according to our test method shown in Fig. 2(b), the frequency of the signal to evaluate the system performance is 76 MHz. It is recorded by a multiple-channel dead-time-free Λ-mode frequency counter (K + K FXE) with a gate time of 1 s and a phase measurement resolution of 12.2 ps. We use both the spooled fiber in the laboratory and the commercial field fiber link to verify our proposed TiLS, TiLRS, and TiRS. The RF sources at the TiLS and TiRS are synchronized to the same time base during the experiment.

B. Phase-Temperature Coefficient Measurement

According to (2), γ can be used to assess the effect of temperature fluctuations on the instability of optical frequency transfer systems. To demonstrate that our proposed system is extremely insensitive to temperature variations, we measure the value of γ using a similar approach in [28].

We first measure the phase-temperature coefficient of the proposed TiLRS in the presence of out-of-loop paths. By not performing the frequency mixing process, only the signal detected in PD3 with the round-trip fiber link-introduced phase noise is employed for the ANC setup, which results in introducing the out-of-loop paths marked by the blue cylinders shown in Fig. 1(b). The fiber-optic components of the TiLRS are housed in a 270 × 166 × 78 mm^3 aluminum box with a built-in thermistor and the corresponding temperature sensing circuit capable of recording temperature fluctuations through a micro-controller. The temperature measurement accuracy reaches 0.01 K, and the sampling time is set to 1 s. TiLS, TiLRS, and TiRS are connected with short fibers and placed in the laboratory environment. Using the ET method shown in Fig. 2(b), the time error can be acquired by converting the frequency deviation of the recorded 76-MHz test signal. The measured time error (blue line, left axis) and the relevant temperature fluctuations in the aluminum box (red line, right axis) over 48 h are shown in Fig. 3(a). It is worth mentioning that, during the test, we control the temperature fluctuations of the environment by periodically turning on and off the air conditioning system in the laboratory, which resulted in a temperature fluctuation range of more than 8 K. Utilizing the multiple linear regression algorithm, the calculated fitting value of γ with the 95% confidence interval is as high as 7.6 *f*s/K, indicating that the out-of-loop path length is about 20.5 cm. In the case of the conventional LRS, as illustrated in Fig. 1(c), the out-of-loop path length may be longer due to the presence of the FM pigtails, which could cause a larger phase-temperature coefficient. While it can be diminished through the implementation of out-of-loop length matching or fiber welding techniques, it is typically constrained to a range of *f*s/K [28], [29], [38].

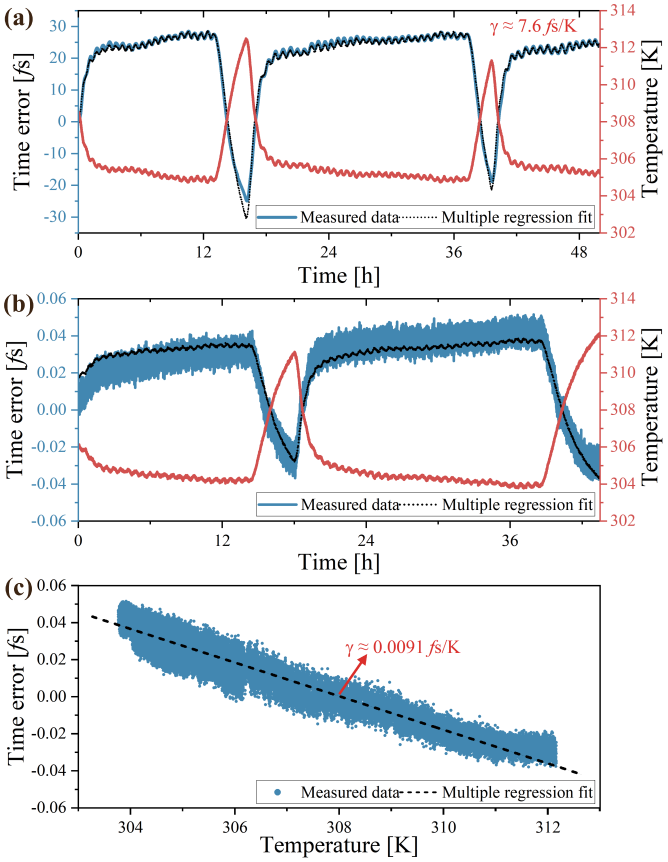

Fig. 3. (a) Measured time error (blue line) of the 76-MHz test signal from the cascaded system with one TiLS, TiLRS, and TiRS carrying the out-of-loop noise, the fit time error (black dotted line) and the temperature fluctuations (red line) as a function of time. (b) Measured time error (blue line) of the 76-MHz test signal from the cascaded system with one TiLS, TiLRS, and TiRS, the fit time error (black dotted line) using the multiple linear regression algorithm and the temperature fluctuations (red line) in the aluminum box equipped with all the fiber-optic components as a function of time. (c) Measured time error (blue dots) and the fit time error (black dotted line) as a function of the temperature fluctuations.

Furthermore, we measure the phase-temperature coefficient of the proposed TiLRS when the out-of-loop noise is compensated. Likewise, we simultaneously measure the time error (blue line, left axis) and the temperature fluctuations in the aluminum box (red line, right axis), and the results are shown in Fig. 3(b). Fig. 3(c) shows the time error results (blue dots)

TABLE I

COMPARISON OF REPRESENTATIVE OPTICAL FREQUENCY TRANSFER SYSTEMS' PHASE-TEMPERATURE COEFFICIENT AND THE RELATED OUT-OF-LOOP NOISE SUPPRESSION METHOD. PLC: PLANAR LIGHTWAVE CIRCUIT

Interferometer type	Out-of-loop noise suppression method	Temperature stabilization	γ	Reference
Fiber-optic	Out-of-loop path in same housing	Active	7 fs/K	[40]
Fiber-optic	Out-of-loop path matching and in same housing	Active	1 fs/K	[28]
Fiber-optic	Out-of-loop path matching and in same housing	Passive	5.55* fs/K	[34]
Fiber-optic	Out-of-loop path reducing and matching	Active	1.35 fs/K	[29]
Photonic integrated	Compact optical waveguide on PLC	Passive	4.66×10^{-2}* as/K	[35]
Free-space	Fiber-optic and free-space hybrid interferometer	Active	not mentioned	[33]
Free-space	All-dielectric free-space interferometer	Passive	0.51* fs/K	[31]
Fiber-optic	Inline out-of-loop noise compensation	Passive	9.1 as/K	This work

*: estimated value

at varying temperatures, exhibiting a discernible linear correlation, as evidenced by (2). The multiple linear regression fitting is also performed with a 95% confidence interval, whereby the γ value is approximately 9.1 as/K, three orders of magnitude lower than the circumstance suffering from the out-of-loop noise, proving that our proposed inline out-of-loop noise detection and compensation method is of great help to reduce the temperature sensitivity of the interferometer. The fit time error using the temperature fluctuation data according to (2) is shown in the black dotted line in Fig. 3(b), showing a fluctuation trend corresponding to the experimental results.

Table I summarizes the evaluated phase-temperature coefficient from the optical frequency transfer systems with different schemes. In comparison to the relay station comprising fiber-optic components, our proposed inline out-of-loop noise detection and compensation method is able to reduce the phase-temperature coefficient by three orders of magnitude, further proving that our proposed TiLRS has the lowest temperature sensitivity so far among the reported fiber-optic interferometers. Note that the estimated γ value of the photonic integrated interferometer demonstrated in [35] is two orders of magnitude lower than our measured result. This discrepancy is attributed to the fact that the photonic integrated interferometer is about two orders of magnitude smaller in size than the conventional fiber-optic devices, which leads to a reduction in the interferometer's noise floor by one to two orders of magnitude and a corresponding enhancement in the phase-temperature coefficient.

C. Performance of the Directly Linked System and the End-to-End Test Method

For the system fractional frequency instability, we first test the characterization of the directly linked system with the TiLS and TiRS as shown in Fig. 2(b). The experiment is implemented inside a laboratory without any temperature control and with temperature fluctuations larger than 8 K. By using the MTWC method, the fractional frequency instability calculated by the 76-MHz test signal in terms of MDEV is shown in Fig. 4. The gray up triangle markers and the red square markers illustrate the fractional frequency instabilities of the directly linked system connected only by the short fiber and the system with a 50-km spooled fiber link, respectively. The noise floor shows a fractional frequency instability of 1.35×10^{-17} at the integration time of 1 s, decreases and reaches approximately 3.13×10^{-21} at the integration time

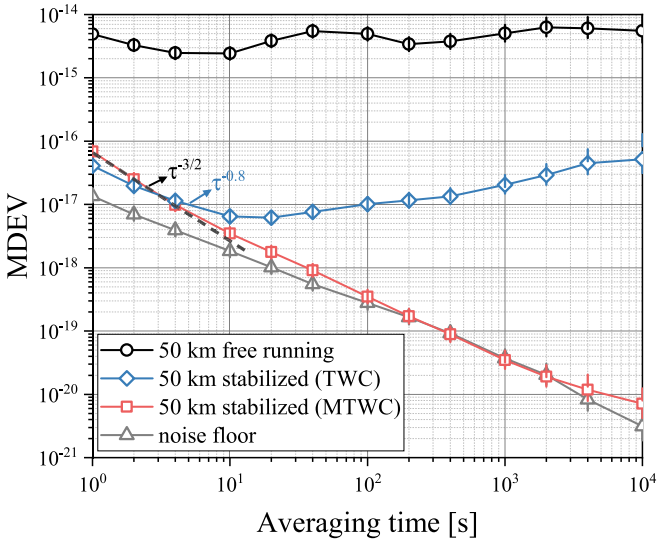

Fig. 4. Measured fractional frequency instabilities of the interferometer noise floor of the directly linked system (gray up triangles), the directly linked system with a 50-km spooled fiber link evaluated by the MTWC method (red squares) and the conventional TWC method (blue diamonds) and a 50-km free running link (black circles).

of 10 000 s. After connecting the TiLS and TiRS with a 50-km fiber link, the fractional frequency instability increases to 6.86×10^{-17} at 1 s and 7.13×10^{-21} at 10 000 s, and the long-term instability can be improved by six orders of magnitude compared to the MDEV results of the free running link (black circle markers). The MDEV results of the stabilized system having a decreasing trend of $\tau^{-3/2}$ for averaging times up to a few seconds, indicating that the residual phase noise is mainly limited by the white phase noise [41]. The measured results show that the proposed novel configurations of TiLS and TiRS as well as the MTWC method are not affected by the temperature fluctuations.

As a contrast, we also evaluate the system with the conventional TWC method. Refer to Fig. 2(c) and (d), the frequency of the two test signals ET1 and ET2 obtained in the TiLS and TiRS is 24 and 176 MHz, respectively. The two signals are also recorded by the same multichannel frequency counter, and carried out the post-processing calculation. The MDEV result is obtained by the difference between ET2 and ET1 by a factor of 2, which is shown by the blue diamond markers in Fig. 4. The MDEV curve obtained through such an evaluation method clearly deviates from the $\tau^{-3/2}$ trend within 10 s,

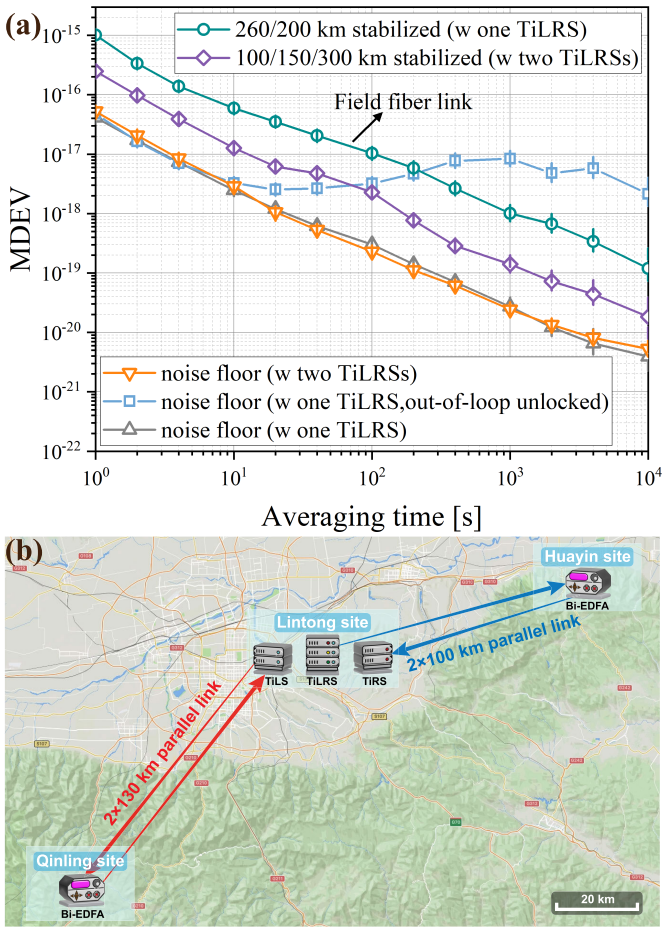

Fig. 5. (a) Measured fractional frequency instabilities of the interferometer noise floor of the cascaded transfer system using one TiLRS with the out-of-loop noise locked (gray up triangles) and unlocked (blue squares), the interferometer noise floor using two TiLRSs (orange down triangles), the stabilized 550-km spooled fiber link (purple diamonds), and the stabilized 460-km commercial field fiber link (green circles). (b) Map of the 460-km cascaded commercial field fiber link consists of the 2 × 130-km parallel link from the Qinling site to Lintong site and the 2 × 100-km parallel link from Lintong site to Huayin site.

approximating a $\tau^{-0.8}$ slope. More importantly, the long-term instability exhibits a significant degradation, worsening by four orders of magnitude compared to the MTWC-based one. Such degradation can be attributed to the introduction of non-white phase noise caused by frequency aliasing during the TWC process. Therefore, even ignoring the influence of the out-of-loop paths, the ET signal chosen in the traditional TWC method cannot accurately assess our proposed system's performance.

D. Performance of the Cascaded System

Subsequently, we further characterize the TiLRS by adding it into the cascaded system. The gray up triangle markers in Fig. 5(a) represent the fractional frequency instabilities of the interferometer noise floor of the cascaded system with one TiLRS, which is about 4.12×10^{-17} at 1 s and 3.91×10^{-21} at 10 000 s. We can see that the phase noise introduced by the phase locking process in the TiLRS will further aggravate the noise floor. As a supplement, we test the MDEV results of floor noise under the same ambient temperature fluctuations when the out-of-loop noise is unlocked (blue square markers). Due to the temperature-induced out-of-loop noise, the long-term instability has been deteriorated by nearly three orders of magnitude. We additionally measured the cascaded system performance with the 550-km spooled fiber link using two TiLRSs (purple diamond markers). The length of the fiber links between the TiLS, two TiLRSs, and the TiRS is set to be 100, 150, and 300 km, respectively. The results show a short-term instability of 2.48×10^{-16} at 1 s and a long-term instability of 1.83×10^{-20} at 10 000 s. Similarly, the slope of the MDEV results with the TiLRSs is also close to $\tau^{-3/2}$ for averaging times up to a few seconds. The deviation of the decreasing trend of the measured fractional frequency instability from the dependency of $\tau^{-3/2}$ may be due to the polarization mode dispersion (PMD) caused by the fiber birefringence. The group velocity delay caused by the PMD is uncorrelated for the forward and backward signals along the fiber link [42], which means that the PMD-induced phase noise cannot be eliminated by the ANC setup. A possible way to suppress the PMD-induced phase noise is to introduce a polarization scrambler before the fiber link [43]. By periodically changing the polarization state of the optical frequency signal, the scrambler can effectively average out the PMD effects. Additionally, by adopting the independent time base at the TiLRSs, we can get the same results with the phase synchronization between each station, proving that the TiLRSs are time base-independent.

We also demonstrate the cascaded optical frequency transfer system with one TiLRS on the commercial fiber link. As shown in Fig. 5(b), the commercial fiber link consists of a 2 × 130-km parallel link from Lintong site to Qinling site and a 2 × 100-km parallel link from Lintong site to Huayin site in Xi'an province, China. The TiLS, TiLRS, and TiRS are all set at the Lintong site for the loopback test. The average attenuation of the fiber links is about 0.25 dB/km, and to compensate for the link loss, two Bi-EDFAs with a gain of approximately 18 and 15 dB are deployed at the Qinling site and Huayin, respectively. According to the green circle markers in Fig. 5(a), the stabilized commercial field fiber link shows a fractional frequency instability of about 1.01×10^{-15} at 1 s and decreases to 1.20×10^{-19} at 10 000 s. To be noted that the phase noise PSD per-unit-length in the commercial fiber link is about 38.5 rad^2/Hz/km in China [44] and the system instability at 1 s is estimated to be 1.07×10^{-15} according to the formula given in [3], which is in good agreement with the test result. Furthermore, the SNR of the in-loop beatnote signals is approximately 33.5 and 37 dB, respectively. According to [45], this may lead to the PLL generating one cycle slip approximately every 9000 s for a filter bandwidth of 10 MHz. Thus, the decreasing trend of the fractional frequency instability could be limited by the unidentified cycle slips as discussed in our previous work [11]. One way to suppress the reduction in the instability caused by cycle slips is to use the Kalman-filter-based algorithm or filter-based technique to identify these cycle slips [46], [47].

Complementary to the time domain characterization, we also evaluate the accuracy of the stabilized cascaded 460-km commercial fiber link. Fig. 6(a) shows the measured

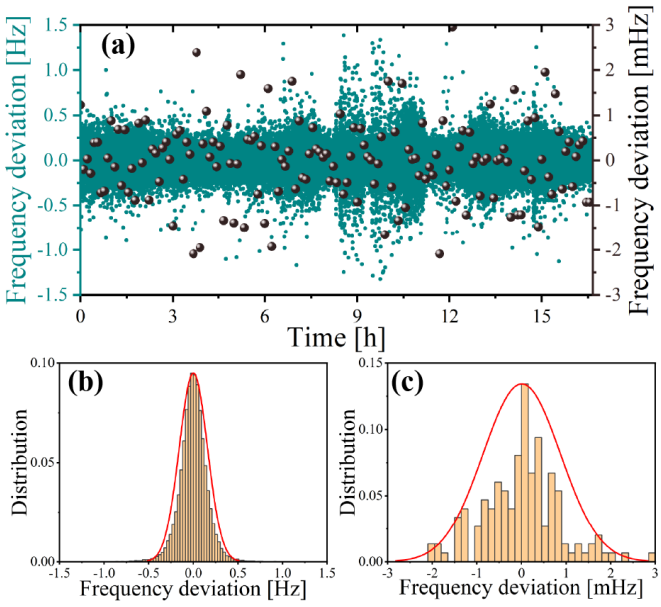

Fig. 6. (a) 59 962 data points taken from the end-to-end test signal for the stabilized cascaded 460-km commercial field fiber link with dead-time free Λ-mode frequency counters with a 1-s gate time (green points, left axis). The unweighted mean values for all cycle-slip free 400-s long segments produce 149 data points (black dots, right axis). (b) Histograms (brown bars) and (c) Gaussian fits (red curves) for 1-s data points and 400-s averages.

frequency deviation of the 76-MHz signal for the stabilized cascaded system with one TiLRS over successive 59 962 s (green point, left axis). We calculated all cycle-slip free 400-s averages (black dots, right axis) to obtain the smallest uncertainty [48], [49]. Fig. 6(b) and (c) presents the histograms (brown bars) and Gaussian fits (red curves) of the frequency deviation for the 59 962 and 149 frequency data, respectively. According to the Gaussian fit in Fig. 6(c), the mean frequency is shifted by 5.39 μHz (2.78×10^{-20}) and the standard deviation of the 400-s averages is 873.07 μHz (3.69×10^{-19}). Taking the long-term instability shown in Fig. 5(a) into account, we can conservatively estimate the accuracy of the transmitted optical signal through the 460-km commercial fiber link as shown in the last data point of the MDEV, resulting in relative frequency accuracy of 1.20×10^{-19}. Thus, we are able to conclude that there is no systematic frequency shift arising in the extraction setup at a level of a few 10^{-19}.

IV. Conclusion

In conclusion, we for the first time demonstrate the TiLS, TiLRS, and TiRS, which do not need any sophisticated temperature control. At the same time, we propose a modified ET method suitable for our proposed system which prevents introducing the additional phase noise coming from the out-of-loop paths. The phase-temperature coefficient of our proposed interferometer structure is about 9.1 as/K and has more than three orders of improvement compared with the conventional temperature-controlled fiber-optic interferometers [28], [29], [38]. Additionally, the effect of the RF noise in each station can be eliminated based on our proposed configurations. The fractional frequency instability for the 550-km cascaded spooled fiber link with two TiLRSs is less than 2.48×10^{-16} at 1 s and 1.83×10^{-20} at 10 000 s. At the same time, for the 460-km commercial fiber link, the fractional frequency instability is 1.01×10^{-15} at the integration time of 1 s and 1.20×10^{-19} at the integration time of 10 000 s. The frequency uncertainty of the optical signal after transferring through the 460-km fiber link relative to that of the reference optical signal is within a few 10^{-19}. This technology drastically reduces the need for the complicated temperature control systems, which is a guideline for the implementation of low-cost, highly reliable, and integrated optical frequency transfer over widespread fiber links.

References

[1] M. Schioppo et al., "Ultrastable optical clock with two cold-atom ensembles," *Nature Photon.*, vol. 11, no. 1, pp. 48–52, Jan. 2017.
[2] W. F. McGrew et al., "Atomic clock performance enabling geodesy below the centimetre level," *Nature*, vol. 564, no. 7734, pp. 87–90, Dec. 2018.
[3] S. Droste et al., "Optical-frequency transfer over a single-span 1840 km fiber link," *Phys. Rev. Lett.*, vol. 111, no. 11, Sep. 2013, Art. no. 110801.
[4] D. Calonico et al., "High-accuracy coherent optical frequency transfer over a doubled 642-km fiber link," *Appl. Phys. B, Lasers Opt.*, vol. 117, no. 3, pp. 979–986, Dec. 2014.
[5] Y. He et al., "Long-distance telecom-fiber transfer of a radio-frequency reference for radio astronomy," *Optica*, vol. 5, no. 2, pp. 138–146, 2018.
[6] C. Clivati et al., "A VLBI experiment using a remote atomic clock via a coherent fibre link," *Sci. Rep.*, vol. 7, no. 1, p. 40992, Feb. 2017.
[7] L. Hu, N. Poli, L. Salvi, and G. M. Tino, "Atom interferometry with the sr optical clock transition," *Phys. Rev. Lett.*, vol. 119, no. 26, Dec. 2017, Art. no. 263601.
[8] C. Lisdat et al., "A clock network for geodesy and fundamental science," *Nature Commun.*, vol. 7, p. 12443, Aug. 2016.
[9] F. Riehle, "Optical clock networks," *Nature Photon.*, vol. 11, no. 1, pp. 25–31, Jan. 2017.
[10] L. Hu, X. Tian, G. Wu, and J. Chen, "Passive optical phase noise cancellation," *Opt. Lett.*, vol. 45, no. 15, p. 4308, 2020.
[11] J. Shen et al., "Multiple-branch optical frequency transfer without the frequency allocation constraints," *J. Lightw. Technol.*, vol. 41, no. 17, pp. 5529–5537, Sep. 1, 2023.
[12] L. Sliwczynski, P. Krehlik, L. Buczek, and M. Lipinski, "Frequency transfer in electronically stabilized fiber optic link exploiting bidirectional optical amplifiers," *IEEE Trans. Instrum. Meas.*, vol. 61, no. 9, pp. 2573–2580, Sep. 2012.
[13] L. Wang, Y. Liu, W. Jiao, L. Hu, J. Chen, and G. Wu, "Fast and on-line link optimization for the long-distance two-way fiber-optic time and frequency transfer," *Opt. Exp.*, vol. 30, pp. 25522–25535, Jul. 2022.
[14] O. Terra et al., "Phase-coherent comparison of two optical frequency standards over 146 km using a telecommunication fiber link," *Appl. Phys. B*, vol. 97, no. 3, pp. 541–551, Nov. 2009.
[15] Z. Qiu, R. Li, L. Hu, G. Wu, and J. Chen, "Optically synchronized unidirectional optical amplifier-based coherent optical fiber links," *Opt. Lett.*, vol. 49, no. 10, p. 2761, 2024.
[16] P. A. Williams, W. C. Swann, and N. R. Newbury, "High-stability transfer of an optical frequency over long fiber-optic links," *J. Opt. Soc. Amer. B, Opt. Phys.*, vol. 125, no. 8, pp. 1284–1293, Jul. 2008.
[17] Q. Zang et al., "Cascaded transfer of optical frequency with a relay station over a 224 km deployed fiber link," *Infr. Phys. Technol.*, vol. 128, Jan. 2023, Art. no. 104511.
[18] J. Kim, H. Schnatz, D. S. Wu, G. Marra, D. J. Richardson, and R. Slavík, "Optical injection locking-based amplification in phase-coherent transfer of optical frequencies," *Opt. Lett.*, vol. 40, no. 18, p. 4198, 2015.
[19] Z. Feng et al., "High-gain optical injection locking amplifier in phase-coherent optical frequency transmission," *IEEE Photon. J.*, vol. 11, no. 1, pp. 1–9, Feb. 2019.
[20] O. Lopez et al., "Cascaded multiplexed optical link on a telecommunication network for frequency dissemination," *Opt. Exp.*, vol. 18, no. 16, p. 16849, 2010.
[21] X. Deng et al., "Coherent phase transfer via fiber using heterodyne optical phase locking as optical amplification," *Appl. Opt.*, vol. 57, no. 32, pp. 9620–9624, 2018.

[22] X. Zhang et al., "All-passive cascaded optical frequency transfer," *IEEE Photon. Technol. Lett.*, vol. 34, no. 8, pp. 413–416, Apr. 4, 2022.

[23] N. Chiodo et al., "Cascaded optical fiber link using the internet network for remote clocks comparison," *Opt. Exp.*, vol. 23, no. 26, p. 33927, 2015.

[24] R. Xue, L. Hu, J. Shen, J. Chen, and G. Wu, "Branching optical frequency transfer with enhanced post automatic phase noise cancellation," *J. Lightw. Technol.*, vol. 39, no. 14, pp. 4638–4645, Jul. 14, 2021.

[25] X. Tian, L. Hu, G. Wu, and J. Chen, "Hybrid fiber-optic radio frequency and optical frequency dissemination with a single optical actuator and dual-optical phase stabilization," *J. Lightw. Technol.*, vol. 38, no. 16, pp. 4270–4278, Aug. 12, 2020.

[26] H. Gao, Y. Jiang, Y. Cui, L. Zhang, J. Jia, and L. Jiang, "Investigation on the thermo-optic coefficient of silica fiber within a wide temperature range," *J. Lightw. Technol.*, vol. 36, no. 24, pp. 5881–5886, Dec. 15, 2018.

[27] G. Adamovsky et al., "Peculiarities of thermo-optic coefficient under different temperature regimes in optical fibers containing fiber Bragg gratings," *Opt. Commun.*, vol. 285, no. 5, pp. 766–773, Mar. 2012.

[28] F. Stefani et al., "Tackling the limits of optical fiber links," *J. Opt. Soc. Amer. B, Opt. Phys.*, vol. 32, no. 5, p. 787, 2015.

[29] Q. Zhou et al., "Robust transfer of optical frequency over 500 km fiber link with instability of 10^{-21}," *Chin. Phys. Lett.*, vol. 41, no. 8, Aug. 2024, Art. no. 084202.

[30] H. J. Kang et al., "Free-space transfer of comb-rooted optical frequencies over an 18 km open-air link," *Nature Commun.*, vol. 10, no. 1, pp. 1–8, Sep. 2019.

[31] T. Jürss, G. Grosche, and S. Koke, "Free-space interferometer design for optical frequency dissemination and out-of-loop characterization below the 10^{-21}-level," *Photon. Res.*, vol. 11, no. 6, pp. 1113–1124, 2023.

[32] L. Hu et al., "Free-space point-to-multiplepoint optical frequency transfer with lens assisted integrated beam steering," *IEEE Trans. Instrum. Meas.*, vol. 71, pp. 1–10, 2022.

[33] E. Cantin, M. Tønnes, R. L. Targat, A. Amy-Klein, O. Lopez, and P.-E. Pottie, "An accurate and robust metrological network for coherent optical frequency dissemination," *New J. Phys.*, vol. 23, no. 5, May 2021, Art. no. 053027.

[34] D. Xu, P. Delva, O. Lopez, A. Amy-Klein, and P.-E. Pottie, "Reciprocity of propagation in optical fiber links demonstrated to 10^{-21}," *Opt. Exp.*, vol. 27, no. 25, pp. 36965–36975, 2019.

[35] T. Akatsuka et al., "Optical frequency distribution using laser repeater stations with planar lightwave circuits," *Opt. Exp.*, vol. 28, no. 7, pp. 9186–9197, 2020.

[36] L. Hu, L. Lu, G. Wu, L. Zhou, and J. Chen, "Silicon circuits for optical frequency transfer," in *Proc. Joint Conf. IEEE Int. Freq. Control Symp. Eur. Freq. Time Forum (EFTF/IFC)*, Oct. 2021, pp. 1–2.

[37] L. Hu, R. Xue, G. Wu, and J. Chen, "Performance of digital servos in an optical frequency transfer network," *Rev. Sci. Instrum.*, vol. 92, no. 5, pp. 1–9, May 2021, Art. no. 053709.

[38] W.-K. Lee, F. Stefani, A. Bercy, O. Lopez, A. Amy-Klein, and P.-E. Pottie, "Hybrid fiber links for accurate optical frequency comparison," *Appl. Phys. B, Lasers Opt.*, vol. 123, no. 5, pp. 161–171, May 2017.

[39] C. E. Calosso et al., "Frequency transfer via a two-way optical phase comparison on a multiplexed fiber network," *Opt. Lett.*, vol. 39, no. 5, pp. 1177–1180, 2014.

[40] O. Lopez, A. Haboucha, B. Chanteau, C. Chardonnet, A. Amy-Klein, and G. Santarelli, "Ultra-stable long distance optical frequency distribution using the Internet fiber network," *Opt. Exp.*, vol. 20, no. 21, pp. 23518–23526, 2012.

[41] S. T. Dawkins, J. J. McFerran, and A. N. Luiten, "Considerations on the measurement of the stability of oscillators with frequency counters," *IEEE Trans. Ultrason., Ferroelectr., Freq. Control*, vol. 54, no. 5, pp. 918–925, May 2007.

[42] D. Xu, O. Lopez, A. Amy-Klein, and P.-E. Pottie, "Non-reciprocity in optical fiber links: Experimental evidence," *Opt. Exp.*, vol. 29, no. 11, pp. 17476–17490, 2021.

[43] D. Xu, O. Lopez, A. Amy-Klein, and P.-E. Pottie, "Polarization scramblers to solve practical limitations of frequency transfer," *J. Lightw. Technol.*, vol. 39, no. 10, pp. 3106–3111, May 8, 2021.

[44] X. Zhang et al., "Passively stable dissemination of ultrastable optical frequency via a noisy field fiber network," *Opt. Laser Technol.*, vol. 157, pp. 1–7, Jan. 2023, Art. no. 108738.

[45] L. C. Sinclair et al., "Invited article: A compact optically coherent fiber frequency comb," *Rev. Sci. Instrum.*, vol. 86, no. 8, pp. 1–15, Aug. 2015.

[46] L. C. Sinclair, H. Bergeron, W. C. Swann, E. Baumann, J.-D. Deschênes, and N. R. Newbury, "Comparing optical oscillators across the air to milliradians in phase and 10^{-17} in frequency," *Phys. Rev. Lett.*, vol. 120, no. 5, pp. 1–6, Jan. 2018, Art. no. 050801.

[47] Z. Qiu et al., "Nearly-continuous kilometer-scale free-space optical frequency comparison in the presence of Doppler shift," *IEEE Trans. Instrum. Meas.*, vol. 73, pp. 1–10, 2024.

[48] E. Benkler, C. Lisdat, and U. Sterr, "On the relation between uncertainties of weighted frequency averages and the various types of Allan deviations," *Metrologia*, vol. 52, no. 4, pp. 565–574, Aug. 2015.

[49] W.-K. Lee, D.-H. Yu, C. Y. Park, and J. Mun, "The uncertainty associated with the weighted mean frequency of a phase-stabilized signal with white phase noise," *Metrologia*, vol. 47, no. 1, pp. 24–32, Feb. 2010.

Ziang Qiu received the B.S. degree from Sichuan University, Chengdu, China, in 2021. He is currently pursuing the Ph.D. degree with the State Key Laboratory of Photonics and Communications, Shanghai Jiao Tong University, Shanghai, China.

His current research interests include optical frequency transfer and photonic integrated chips.

Zijie Zhou received the B.S. degree in electronic information engineering from the University of Science and Technology of China, Anhui, China, in 2022. He is currently pursuing the Ph.D. degree with the State Key Laboratory of Photonics and Communications, Department of Electronic Engineering, Shanghai Jiao Tong University, Shanghai, China.

His current research interests include ultrastable lasers and optical frequency comparison.

Liang Hu (Member, IEEE) received the B.S. degree from Hangzhou Dianzi University, Hangzhou, China, in 2011, the M.S. degree from Shanghai Jiao Tong University, Shanghai, China, in 2014, and the Ph.D. degree from the University of Florence, Florence, Italy, in 2017.

During which he was a Marie-Curie Early Stage Researcher at FACT project. He is currently a Tenure-Track Assistant Professor in the State Key Laboratory of Photonics and Communications, Department of Electronic Engineering, Shanghai Jiao Tong University. His current research interests include photonic signal transmission and atom interferometry.

Jiao Liu received the B.S. degree from the School of Information Engineering, Xi'an University, Xi'an, China, in 2012, and the M.S. degree from the School of Physics and Technology, Suzhou University of Science and Technology, Suzhou, China, in 2015.

In 2016, she joined with the Department of Electronic Engineering, Shanghai Jiao Tong University, Shanghai, China, where she is currently an Engineer. Her research interests include silicon photonic devices and photonic time and frequency transfer.

Guiling Wu (Member, IEEE) received the B.S. degree from Harbin Institute of Technology, Harbin, China, in 1995, and the M.S. and Ph.D. degrees from Huazhong University of Science and Technology, Huazhong, China, in 1998 and 2001, respectively.

He is currently a Professor with the State Key Laboratory of Photonics and Communications, Department of Electronic Engineering, Shanghai Jiao Tong University, Shanghai, China. His current research interests include photonic signal processing and transmission.

Jianping Chen received the B.S. degree from Zhejiang University, Hangzhou, China, in 1983, and the M.S. and Ph.D. degrees from Shanghai Jiao Tong University, Shanghai, China, in 1986 and 1992, respectively.

He is currently a Professor with the State Key Laboratory of Photonics and Communications, Department of Electronic Engineering, Shanghai Jiao Tong University. He is a Principal Scientist of National Basic Research Program of China (also known as 973 Program). His main research interests include opto-electronic devices and integration, photonic signal processing, and system applications.

Xiang Zhang is currently pursuing the Ph.D. degree with the Key Laboratory of Time and Frequency Benchmarks, University of Chinese Academy of Sciences, Beijing, China.

His current research interests include photonic signal transmission and atom interferometry.

Ruifang Dong received the B.Eng. degree in opto-electronics and the M.S. degree in optics from Shanxi University, Taiyuan, China, in 1998 and 2001, respectively, and the Ph.D. degree in physics from Friedrich-Alexander-University of Erlangen-Nuremberg, Erlangen, Germany, in 2009.

From 2009 to 2010, she was a Post-Doctoral Researcher with the Max Planck Institute for the Science of Light, Erlangen, and then the Technical University of Denmark, Denmark. Since 2011, she has been a Professor with the National Time Service Center, Chinese Academy of Sciences, Beijing, China.

Tao Liu received the B.S. degree in optoelectronics information engineering and the Ph.D. degree in optical engineering from Huazhong University of Science and Technology, Wuhan, China, in 2015 and 2021, respectively.

His research was focused on fiber grating laser sensor and high-resolution distributed acoustic sensor.

Shougang Zhang received the Ph.D. degree in quantum physics from the Université Pierre et Marie Curie, Paris, France, in 2004.

From 1993 to 1997, he was an Assistant Researcher with the National Institute of Metrology, Beijing, China. Since 2005, he has been the Director and the Chief Researcher with the Quantum Frequency Standard Laboratory, National Time Service Center, Chinese Academy Sciences, Xi'an, China, where he is currently the Institute Director. His research interests include quantum frequency standard, time and frequency transfers, and quantum physics.